Available online at www.sciencedirect.com
ScienceDirect
Journal of Power Sources 174 (2007) 103–113
JOURNAL OF POWER SOURCES
www.elsevier.com/locate/jpowsour

Synthesis and properties of novel HMS-based sulfonated poly (arylene ether sulfone)/silica nano-composite membranes for DMFC applications

Jie-Cheng Tsai, Jen-Feng Kuo, Chuh-Yung Chen *

Department of Chemical Engineering, National Cheng-Kung University, Tainan 70148, Taiwan

Received 19 July 2007; received in revised form 27 August 2007; accepted 30 August 2007
Available online 4 September 2007

Abstract

Novel 4,4′-dihydroxy-α-methylstilbene (HMS)-based sulfonated poly(arylene ether sulfone) with sulfonic acid composition ranging from 10 to 40 mol% was synthesized via nucleophilic step polymerization of 4,4′-dihydroxy-α-methylstilbene, 4,4′-dichloro-3,3′-disulfonic acid diphenylsulfone and 4,4′-dichlorodiphenylsulfone and blended with silica sol to form organic/inorganic nano-composite membranes. The organic/inorganic nano-composite copolymers produced show a high glass transition temperature and thermal decomposition temperatures from 318 to 451 °C. The copolymers present appropriate toughness during the membrane process. The equilibrium water uptake and proton conductivity of the obtained organic/inorganic nano-composite membranes were measured as functions of temperature, degree of sulfonation and silica content. In general, the water uptake increased from 8 to 37 wt.%, and the proton conductivity of the organic/inorganic nano-composite membranes increased from 0.003 to 0.110 S cm^{-1} as the degree of sulfonation increased from 10 to 40 mol%, the silica content increased from 3 to 10 wt.%, and the temperature increased from 30 to 80 °C. The single cell performance of the 40 mol% organic/inorganic nano-composite membrane with various silica contents ranged from 11 to 13 mW cm^{-2} at 80 °C, and the power density was higher than Nafion® 117. Including the thermal properties, swelling, conductivity and single cell performance, the nano-composite membranes are able to satisfy the requirements of proton exchange membranes for direct methanol fuel cells (DMFC).

Keywords: Proton exchange membrane; Organic/inorganic nano-composite membrane; HMS; Poly(arylene ether sulfone); Direct methanol fuel cell (DMFC)

1. Introduction

In order to decrease emissions of harmful pollutants from fossil fuels and suppress global warming [1], fuel cells have attracted significant attention because of their ability to produce energy with higher efficiency than a turbine. Fuel cells represent a promising energy source for portable devices, automobiles, and stationary appliances [2]. The proton exchange membrane is one of the key components in a fuel cell system. Because of their importance in fuel cells, sulfonated polymer electrolytes have received considerable attention over the last few years. Proton exchange membranes have to satisfy several demanding requirements: proton conductivity higher than 0.1 S cm^{-1}, long-term stability under humidified and heated conditions, and very low permeability to fuel (methanol or hydrogen).

Perfluorosulfonic acid membranes such as Nafion®, with fluoroalkyl ether side chains and sulfonic acid end groups, are the most commonly used material. However, Nafion® membranes have some drawbacks [3]: (i) Nafion® is too expensive and difficult to process; (ii) there is a strong dependence on relative humidity in maintaining the proton conductivity of Nafion® membranes. This is the reason why proton conductivity decreases with dehydration at high temperature; (iii) thermal instability at high temperature. This property causes the membrane to physically shrink during high temperature operation, with subsequent poor contact and proton conductivity between the membrane and the electrodes; (iv) high methanol permeability, which not only wastes fuel but also reduces cell performance for application in direct methanol fuel cells (DMFC).

Over the past few years, several efforts have been made by various academic and industrial groups to replace the

* Corresponding author. Tel.: +886 6 2757575x62643; fax: +886 6 2360464.
E-mail address: ccy7@ccmail.ncku.edu.tw (C.-Y. Chen).

0378-7753/$ – see front matter © 2007 Elsevier B.V. All rights reserved.
doi:10.1016/j.jpowsour.2007.08.086

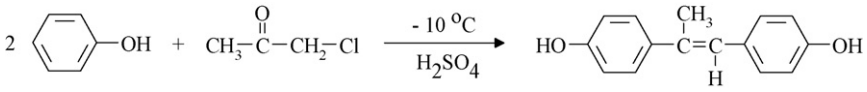

Scheme 1. The reaction for synthesis of the HMS monomer.

Nafion® membranes in fuel cells by cheaper and ecologically more acceptable materials. The approaches of optimization and development of proton exchange membranes have mainly involved synthesis of new hydrocarbon-based aromatic polymer membranes such as sulfonated polybenzimidazole (PBI) [4,5], poly(ether sulfone) (PES) [6–9], poly (ether ether ketone) (PEEK) [10,11], and polyimide (PI) [12]. However, proton exchange membranes based on these polymers suffer from excessive swelling of aromatic polymers, loss of proton conductivity due to degradation of sulfonic acid groups at high temperature, and overall low proton conductivity [13]. For membrane applications, composite membranes consisting of these polymer backbones and inorganic materials have also been studied because of controllable chemical and physical properties produced by combining different components [14–17]. The organic/inorganic nano-composite membranes have attracted great attention because of their dual functionality like specific chemical reactivity and flexibility of the organic polymer backbone, as well as the mechanical properties and thermal stability of the inorganic backbone. The introduction of a finely dispersed inorganic phase has been demonstrated to be successful in controlling selectivity and permeability for gas separation, decreasing compaction, and swelling.

Sulfonated PES have been extensively studied and also tested for fuel cell applications. Membranes made of these compounds possess many good attributes such as good mechanical properties, high heat distortion temperature, good heat-aging resistance, environmental endurance and good processing capacity. The proton conductivity of sulfonated PES membranes was reportedly as high as 10^{-2} S cm^{-1} at 80 °C. In addition, sulfonated PES membranes have lower gas permeability and liquid (water and methanol) permeability than Nafion® [9,18]. In Ueda's study [19], the sulfonated PES cast membranes were somewhat brittle even when using the isopropylidene moiety to provide flexibility. In the present study, a novel sulfonated PES blended with silica sol was used to form organic/inorganic nano-composite membranes. The sulfonated PES membranes were prepared via the direct polymerization method suggested by McGrath and coworkers [8,9,20] to introduce 4,4′-dihydroxy-α-methylstilbene (HMS) monomer, which constitutes an interesting core and which can be prepared in a simple and relatively inexpensive way [21–24]. The nonplanar *trans*-stilbene derivative exhibits a lower melting point and high solubility, overcoming the brittle weakness in growing molecules. The introduction of finely dispersed inorganic silica particles was expected to improve thermal stability, swelling, water content, conductivity and single cell performance with no sacrifice for mechanical property. The resulting HMS-based sulfonated organic/inorganic nano-composite copolymers with different degrees of sulfonation and silica content were characterized by Fourier transform infrared spectroscopy, proton nuclear magnetic resonance spectroscopy, differential scanning calorimetry, thermo-gravimetric analysis, water uptake, proton conductivity, scanning electron microscopy, and DMFC single cell performance. It was expected that the novel HMS-based sulfonated organic/inorganic nano-composite membranes would have suitable properties for fuel cell applications.

2. Materials and experimental

2.1. Materials

Fuming sulfuric acid (30% SO_3) was obtained from Aldrich Chemical Corp. Chloroacetone was purchased from Janssen Chimica Corp. Phenol and sodium hydroxide were obtained from Shimakyo's Pure Chemicals Corp. 4,4′-Dichlorodiphenylsulfone, *N*-methylpyrrolidone (NMP) and toluene were from Acros Corp. Silica sol was obtained from Nissan Chemical Industries Ltd. DMAc and isopropyl alcohol (IPA) were from Mallinckrodt Corp. All reagents were used as received without further purification.

2.2. Monomer synthesis

2.2.1. 4,4′-Dihydroxy-α-methylstilbene (HMS)

HMS was synthesized by the procedure outlined by Zaheer et al. and our previous research [21–24]. Chloroacetone (0.3 mol) and phenol (0.6 mol) were charged into a four-necked Pyrex reactor with stirring and maintained at a constant temperature of −10 °C. Concentrated H_2SO_4 (0.3 mol) was then added dropwise to the solution (Scheme 1). The reaction was considered complete when the viscous product could no longer be stirred. The crude product was re-crystallized from ethanol/water solution, extracted with benzene and washed with petroleum ether; mp 183–184 °C, yield: 21%.

^{1}H NMR (DMSO-d_6): $\delta = 2.1$ (S, 3H, –CH_3), 6.6 (S, 1H, –C=CH–), 6.7 (d, four aromatic protons, o to –OH), 7.1 (d, two aromatic protons, o to –CH_3), 7.3 (d, 2 aromatic protons, o to =CH), 9.4 (s, 2H, –OH).

2.2.2. Sulfonated dichlorodiphenolsulfone (SDCDPS)

The synthesis of SDCDPS was performed according to the procedure reported by McGrath and coeorkers [25–28]. DCDPS (0.099 mol) was dissolved in 60 mL of fuming sulfuric acid (30% SO_3). The solution was stirred at 120 °C for 3 h, then cooled to room temperature and poured into ice water. Sodium chloride was added to precipitate the white crude material. The crude material was then redissolved in deionized water and neutralized with sodium hydroxide solution. It was again precipitated with addition of sodium chloride, filtered, and then recrystallized from IPA/water mixture to afford the highly purified monomer grade SDCDPS, yield: 82%.

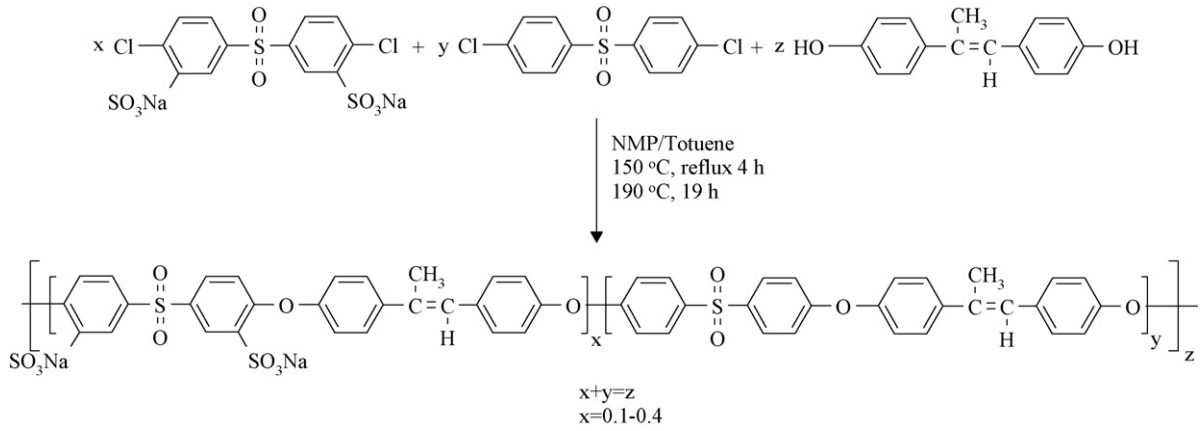

Scheme 2. The synthesis of HMS-based sulfonated PES was prepared via an aromatic nucleophilic substitution reaction for degree of sulfonation from 10 to 40 mol %.

^{1}H NMR (DMSO-d_6): $\delta = 7.6$ (d, two aromatic protons, *m* to $-SO_2$), 7.8 (dd, two aromatic protons, *o* to $-SO_2$), 8.3 (d, two aromatic protons, *o* to $-SO_3Na$).

2.3. Polymer synthesis

HMS-based sulfonated PES was synthesized via an aromatic nucleophilic substitution reaction with SDCDPS, DCDPS, and HMS monomers in NMP with toluene as azeotroping agent (Scheme 2). The degree of sulfonation is the number of disulfonic acid groups per repeating unit. In the reaction, the degree of sulfonation was 10, 20, 30, and 40 mol%. The detailed synthesis of the 10 mol% sulfonated copolymer (HMSHS10), containing 10 mol% SDCDPS and 90 mol% DCDPS, was as follows. The polymerization was carried out in a 150-mL three-necked flask equipped with a mechanical stirrer, nitrogen inlet, and Dean–Stark trap as a reflux condenser. HMS (17.6991 mmol), SDCDPS (1.7699 mmol), and DCDPS (15.9292 mmol) were added, as well as an excess of anhydrous potassium carbonate (20.3540 mmol). NMP (27.2 mL) and toluene (13.6 mL) were then charged into the flask, added as an azeotroping agent. The reaction mixture was refluxed at 150 °C for 4 h to dehydrate the system until water was removed from the reaction. The temperature was raised slowly to 190 °C for 19 h by the controlled removal of the toluene. Then the reaction was cooled to room temperature. The polymer solution was diluted with DMAc, filtered to remove the sodium salt, and precipitated into IPA. The resulting polymer was isolated, washed repeatedly with deionized water to completely remove the residual sodium until the pH reached 6–7, and dried in a vacuum oven at 120 °C for 24 h. The yields of all copolymers were greater than 98%. The HMS-based PES in sodium form was treated with 1 M H_2SO_4 at room temperature for 24 h to give the acid form, and dried in a vacuum oven at 120 °C for 24 h. Silica sol (3, 5 or 10 wt.%) was added to the acid form HMS-based PES solution dissolved in DMAc. The resulting solution was stirred with a magnetic bar for 1 h, and then shaken in an ultrasonic tank for 1 h. The solution was poured onto a Teflon plate and heated to dryness. After cooling to room temperature, the resulting membranes were peeled off.

2.4. Proton nuclear magnetic resonance spectroscopy (^{1}H NMR)

The monomer structures and HMS-based sulfonated PES compositions in the sodium form were obtained from DMSO-d_6 solution (10%, w/v) at room temperature. ^{1}H NMR spectra were measured on a Varian Unity 600 spectrometer using a Bruker AMX 600 MHz.

2.5. Fourier transform infrared spectroscopy (FT-IR)

HMS-based sulfonated PES was dissolved in DMAc (5%, w/v) solution and dropped onto a KBr specimen to form a thin film. Spectra were recorded in the sodium form with a Bio-Rad, FTS-40A spectrometer at room temperature in the range 400–4000 cm^{-1}.

2.6. Scanning electron microscopy (SEM)

SEM micrographs were taken to evaluate the uniformity of the dispersion of added silica in the membranes and the silica particle size. The morphology of the organic/inorganic nano-composite membranes was observed with a Hitachi S4200 field emission scanning electron microscope, which was equipped with an energy dispersive X-ray (EDX) spectrometer to obtain the Si and S ratio in the cross-section.

2.7. Thermo gravimetric analysis (TGA)

The dynamic TGA experiments of the organic/inorganic nano-composite copolymers were run from 100 to 800 °C at a heating rate of 10 °C min^{-1} under a nitrogen atmosphere. Thermo gravimetric analysis measurements were made using a TA instrument TGA Q50.

2.8. Differential scanning calorimetry (DSC)

Thermal analysis of the organic/inorganic nano-composite copolymers was carried out in a Dupont DSC 2910 differential scanning calorimeter at a heating rate of 10 °C min^{-1} from

30 to 300 °C. The freezing water content of the membranes was measured by soaking the membranes in deionized water in the equilibrium state, then the fully hydrated membranes were transferred immediately to seal in an aluminum sample pan, and measured with a heating rate of 2 °C min^{-1} over the range from −30 to 30 °C.

2.9. Water uptake of membranes

Before the measurement of equilibrium water uptake of the organic/inorganic nano-composite membranes, they were dried in a vacuum at 120 °C until constant weight, and that weight noted. The equilibrium water uptake for the membranes was obtained by immersing them in deionized water at room temperature, and the amount of water uptake was measured at predetermined time intervals until constant weight was attained. The weight of equilibrium water uptake of the membranes was determined as follows:

$$\text{water uptake } (\%) = \frac{W_{\text{wet}} - W_{\text{dry}}}{W_{\text{dry}}} \times 100\% \quad (1)$$

where W_{wet} and W_{dry} are the weights of the wet and dry membranes, respectively.

2.10. Proton conductivity measurement

The proton conductivity of the organic/inorganic nano-composite membranes was measured with an electrochemical cell. The cell was placed inside a thermostat in an Ar atmosphere. Impedance analysis was recorded from 30 to 80 °C using an Autolab PGSTAT 30 (Eco Chemie B.V., Netherlands) with frequency response analysis (FRA) software using an oscillation potential of 10 mV from 100 kHz to 10 Hz in a thermostatic cell. The proton conductivity of organic/inorganic nano-composite membranes was determined as follows:

$$\sigma = \frac{l}{RA} \quad (2)$$

where σ is the proton conductivity, l the membrane thickness, R the membrane resistance obtained from impedance analysis, and A is the membrane area, respectively.

2.11. Single cell performance

The organic/inorganic nano-composite membranes were used as proton exchange membranes. The anode electrode used 1.2 mg cm^{-2} Pt/Ru black as catalyst, and the cathode electrode used 0.6 mg cm^{-2} Pt/Ru black. The electrode area was 3.24 cm^2. The cell was heated up to 80 °C, and preheated 2 M methanol solution was pumped into the anode diffusion layer at 100 mL h^{-1}, while oxygen was pumped at 100 mL min^{-1} to the cathode.

3. Results and discussion

3.1. Copolymer characteristics

^{1}H NMR spectroscopy has been employed to provide structural confirmation of the synthesized HMS-based sulfonated copolymers (HMSHS). For this research, NMR has also allowed the structural and compositional determination of sulfonated copolymer segments in the sodium form. By integration and rationing of known reference protons in the polymer, the relative compositions of the series of sulfonated copolymers can be determined. The two protons ortho to the sulfone and adjacent to the sulfonate group (proton 'k', ~8.30 ppm) on the sulfonated dihalide monomer were well separated from aromatic protons of the HMS monomer (proton 'b, b', ~7.63 and 7.45 ppm) on the non-sulfonated segment. These indicate that the sulfonate groups were successfully introduced into the copolymers via a nucleophilic step polymerization without any side reactions. The ^{1}H NMR spectrum for HMSHS20 shown in Fig. 1 is a representative ^{1}H NMR spectrum with 20 mol% sulfonated dichlorodiphenyl sulfone. The integration area revealed that 10, 20, 31, and 41 mol% of sulfonated dichlorodiphenyl sulfone

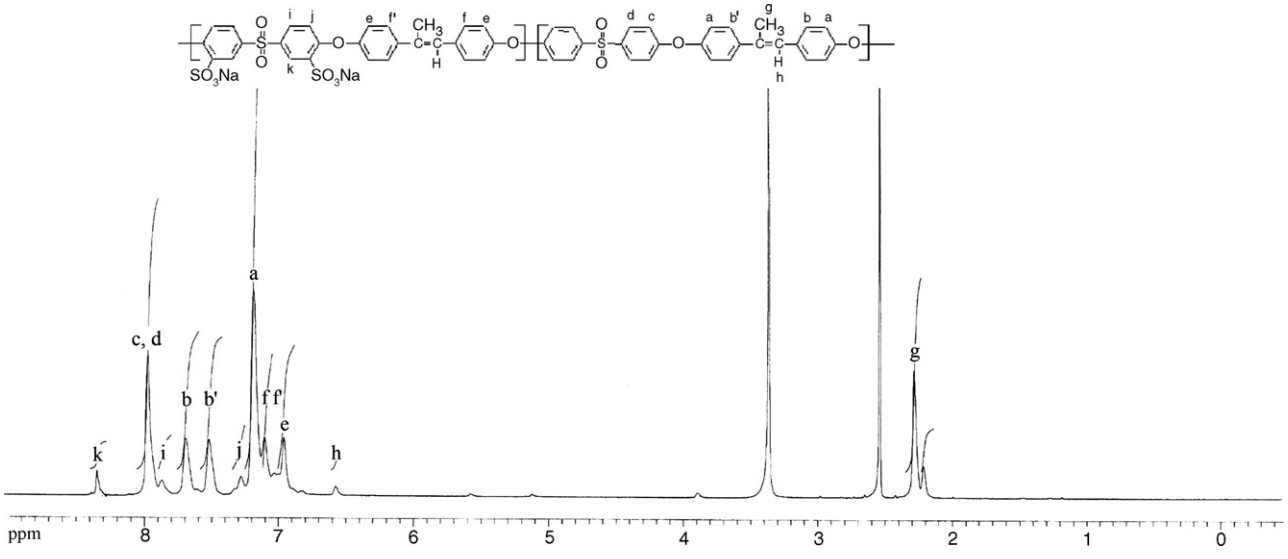

Fig. 1. The ^{1}H NMR spectrum for the HMSHS20 ($x = 0.2$).

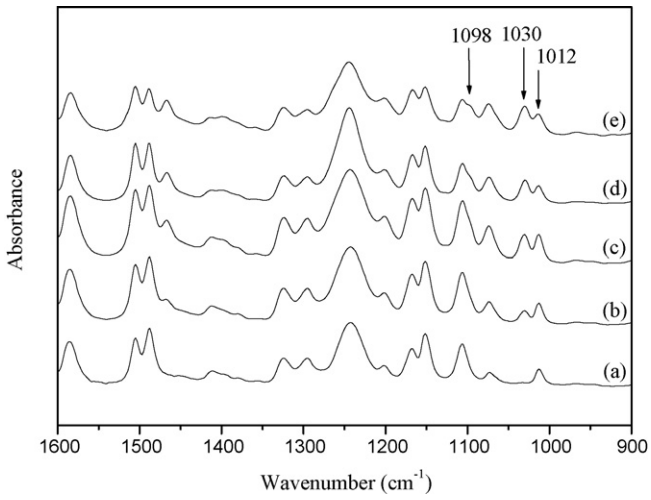

Fig. 2. FT-IR spectra for the HMS-based sulfonated copolymers: (a) HMSHS0 (b) HMSHS10, (c) HMSHS20, (d) HMSHS30, and (e) HMSHS40.

was incorporated into the polymers. The values are in close agreement with those expected from the monomer feed ratio. Similar integrations and calculations were performed for other sulfonated poly (arylene ether sulfones) [27,28].

The FT-IR spectra for the HMSHS are shown in Fig. 2. It was observed that the absorption intensity of the sodium form sulfonate groups (–SO_3Na) at 1030 and 1098 cm^{-1} increased with increasing degree of sulfonation of the copolymers. The copolymer spectra were normalized using the absorption of the Ar–O–Ar linkage at 1012 cm^{-1} in the copolymer backbone. There was an obvious increase in intensity of sodium form sulfonate groups, and the strong characteristic peaks at 1030 and 1098 cm^{-1} were assigned to symmetric and asymmetric stretching of sulfonate groups, respectively, which were observed for all copolymers with loading of sulfonate group composition. The intensity of these two characteristic peaks increased as the content of the sulfonate groups increased from 0 to 40 mol% [8,28]. The symmetric stretching of sulfonate groups at 1030 cm^{-1} can be compared to the in-chain diphenyl ether absorption. All results clearly indicate that the sulfonate groups were qualitatively incorporated into the copolymer without any side reaction and the degree of sulfonation could easily be controlled by varying the molar ratio of the DCDPS and SDCDPS monomers. Quantitative studies of FT-IR spectra are shown in Fig. 3. A linear relationship existed between the degree of sulfonation and the density ratio of sulfonate stretching (1030 cm^{-1}) to diphenyl ether bands (1012 cm^{-1}). The result proved that the sulfonate groups were indeed quantitatively introduced into the copolymers as expected, as shown in other sulfonated poly (arylene ether sulfones) [8].

3.2. Morphology

Scanning electron microscopy (SEM) was used to study the different morphologies of the nano-composite membranes. The cross-section morphology in SEM micrographs of HMSHS20/silica and HMSHS40/silica with varying silica content is illustrated in Fig. 4. The white points represent the electron-dense silica phase. The phase contrast observed under magnification was 30,000 for all nano-composite membranes. From the appearance of SEM micrographs as shown in Fig. 4(a)–(d), non-uniform dispersion and aggregation of the SiO_2 particles shown in the HMSHS20/silica led to large average particle sizes >50 nm. With an increase in sulfonic acid content to HMSHS40/silica, as shown in Fig. 4(e)–(h), the silica particles were well dispersed and revealed relatively small particle size <50 nm. In all nano-composite membranes, silica particles were embedded in the polymer matrix, and this indicated a stronger interaction. This could be expected to reduce the methanol permeability. Due to the cage effects of the clusters of sulfonic acid groups, the increase in sulfonic acid content gave a more uniform dispersion in HMSHS30/silica and HMSHS40/silica than in HMSHS10/silica and HMSHS20/silica composite membranes. The relatively large particle size and non-uniform dispersion of silica in HMSHS10/silica and HMSHS20/silica led to more voids and more freezing water in the membranes, which gave a decrease in conductivity. HMSHS30/silica and HMSHS40/silica had much more cage effects from the clusters of sulfonic acid groups, relatively small particle size and uniform dispersion in the membranes giving an increase in conductivity and decrease in freezing water from 0% to 5% silica, while 10% silica content gave the opposite effect similar to HMSHS10/silica and HMSHS20/silica. The atomic composition analysis by energy dispersive X-ray (EDX) on the cross-section of HMSHS40/silica with varying silica content is shown that the ratio of Si to S was approximately 17:83, 24:76 and 38:62 (wt.%/wt.%), with increasing silica content from 3% to 5% to 10%, respectively.

3.3. Thermal characteristics

The thermal stability of the organic/inorganic nano-composite copolymers was investigated by TGA in sodium and acid forms containing 3, 5 and 10 wt.% silica. The influences of the degree of sulfonation and silica content on 5 wt.% loss temperature (T_{d5}) are summarized in Table 1. Controlled copolymer

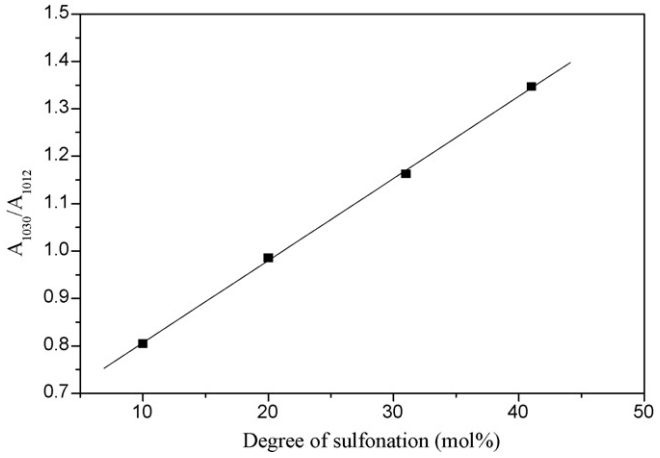

Fig. 3. Quantitative studies of FT-IR spectra compared the density ratio of sulfonate stretching (1030 cm^{-1}) to diphenyl ether bands (1012 cm^{-1}) from HMSHS10 to HMSHS40.

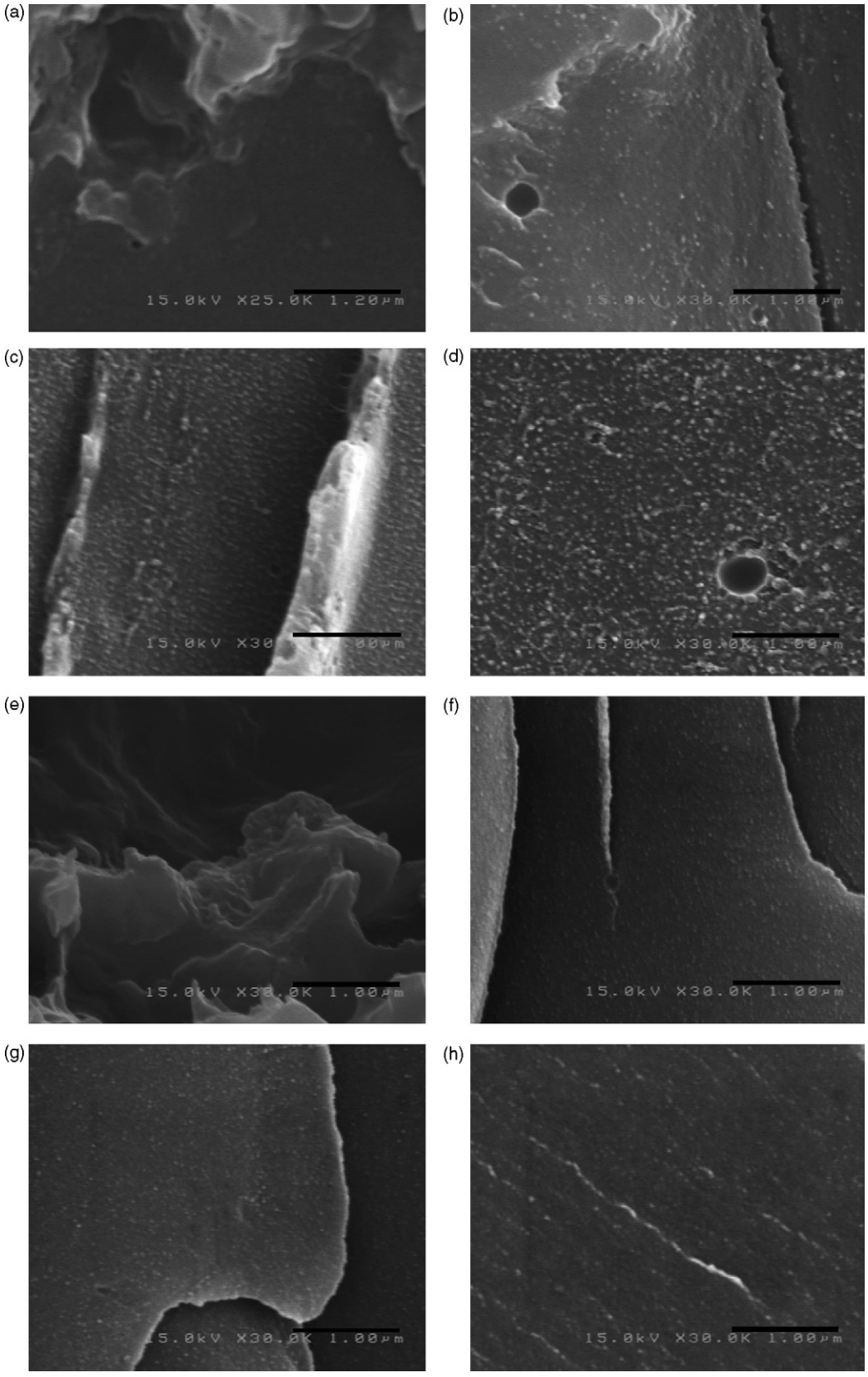

Fig. 4. The cross-section morphology of SEM micrographs: (a) HMSHS20/0% (b) HMSHS20/3%, (c) HMSHS20/5%, (d) HMSHS20/10%, (e) HMSHS40/0%, (f) HMSHS40/3%, (g) HMSHS40/5%, and (h) HMSHS40/10%.

Table 1
The 5 wt.% loss temperature (T_{d5}) of the HMSHS/silica nano-composite copolymers

	Thermal degradation, T_{d5} (°C)			
	0% silica	3% silica	5% silica	10% silica
HMSHS10	433	436	441	451
HMSHS20	351	376	387	399
HMSHS30	333	337	341	344
HMSHS40	318	327	329	334

is well known to be a thermally stable polymer and shows a T_{d5} of 467 °C. All of the sodium form sulfonated copolymers from HMSHS10 to HMSHS40 showed only one weight loss step at around 460 °C, which was assigned to the degradation of the copolymer main chain. Acid form sulfonated copolymers revealed lower T_{d5} values at 433, 351, 333, and 318 °C, which was assigned to the loss of $–SO_3H$ groups by evolution of SO and SO_2. This indicates that the degradation of acid form polymers starts from the desulfonation of sulfonic groups. It was observed in Table 1 that the feature shifted to higher temperatures with increased silica loading. In HMSHS40/silica nano-composite membranes, the temperature substantially increased to 318, 327, 329 and 344 °C with 0%, 3%, 5%, and 10% silica, respectively. This confirmed the phenomena observed by Deng et al. [29]. The improvement in thermal stability for high temperature applications is attributed to the inhibition of SO_2 evolution due to immobilization in the copolymer by silica cages.

Differential scanning calorimetry analysis was used to characterize the thermal transition for the organic/inorganic nano-composite HMSHS. Table 2 summarizes the glass transition temperatures in sodium and acid form. It clearly shows that only one glass transition temperature (T_g) is present in sodium and acid copolymers of HMSHS10 to HMSHS40. Table 2 shows the sodium form as a function of the degree of sulfonation. These DSC data showed an increase in T_g (220, 239, 243, and 258 °C) in the range 10 to 40 mol% of sulfonate groups. The sulfonated acid copolymers also had an increase in T_g (189, 204, 213, and 224 °C) in the set of copolymers. The reason for this is that the bulky substitution of the sodium form hindered the internal rotation, leading to higher glass transition temperatures for the sodium form of sulfonated copolymers than the acid forms. The presence of polar groups such as sulfonate groups produced much more intermolecular interaction and the loading of silica increased the molecular bulkiness of the copolymer chain unit. Both effects hindered the internal rotation, leading to increased glass transition temperatures and obscure for DSC analysis.

Table 2
The glass transition temperatures in sodium and acid form of HMSHS

	Glass transition temperature, T_g (°C)			
	HMSHS10	HMSHS20	HMSHS30	HMSHS40
Sodium form	220	239	243	258
Acid form	189	204	213	224

Table 3
The water uptake of the HMSHS/silica nano-composite membranes

	Water uptake (%)			
	0% silica	3% silica	5% silica	10% silica
HMSHS10	13	10	9	8
HMSHS20	16	14	12	11
HMSHS30	27	26	23	21
HMSHS40	37	36	35	33

3.4. Water uptake

It is well known that water uptake is very important because proton conductivity and mechanical stability are strongly related to the presence of water in membranes. In the presence of water, the hydrophilic part is hydrated, which provides good proton conductivity. The hydrophobic part provides the membranes with good morphological and mechanical stability. On the one hand, an adequate degree of water uptake is desired to maintain good proton conductivity; on the other hand, water uptake should be minimized to provide the membranes with mechanical stability. So controlling polymer membranes with appropriate levels of water uptake is very important. The water uptake of the HMSHS/silica nano-composite membranes is related to the degree of sulfonation and the silica content. The water uptake of the HMSHS membranes was increased with increase in the degree of sulfonation as shown in Table 3. This is due to the fact that the sulfonic acid groups are hydrophilic and hence the membranes with higher sulfonation can absorb more water. Table 3 shows that the water uptake of HMSHS membranes increased from 13% for HMSHS10 to 37% for HMSHS40 at room temperature. There was a sharp increase in the HMSHS30 membrane from lower sulfonation levels. This was perhaps due to the formation of ion clusters. When the sulfonic acid groups were more abundant, the dispersed sulfonic acid groups can form ion clusters, which are hydrophilic and mainly responsible for water uptake [8,9]. All of the HMSHS membranes had water uptake below 40% and maintained their dimensional shape and mechanical strength. It was noteworthy that compared with Nafion® 117 (IEC = 1.73 mmol cm^{-3}), which had a higher water uptake of 30% at room temperature, HMSHS30 membrane had a similar water uptake of 27% with a lower percentage of sulfonic acid groups (1.60 mmol cm^{-3}). The comparison of IEC with water uptake could be converted to a volume base to allow for a more appropriate comparison.

The water uptake of the HMSHS/silica nano-composite membranes decreased with increase in silica content in HMSHS40 (>4 wt.%), because inorganic nano-particles increased the bulkiness and reduced the swelling ability in the copolymer chains [30]. These results indicate that the water uptake, which is significantly related to the methanol crossover, can be controlled by the addition of nano silica particles.

3.5. State of water in the membranes

The water content of the HMSHS/silica nano-composite membranes and Nafion® 117 are summarized in Table 4. Gen-

Table 4
The water content based on total weight of the HMSHS/silica nano-composite membranes and Nafion® 117

	Water content (%)		
	Total	Freezing	Bound
HMSHS10/0%	11.5	0.2	11.3
HMSHS10/3%	9.1	0.3	8.8
HMSHS10/5%	8.3	0.3	8.0
HMSHS10/10%	7.4	0.3	7.1
HMSHS20/0%	13.8	0.2	13.6
HMSHS20/3%	12.3	0.3	12.0
HMSHS20/5%	10.7	1.1	9.6
HMSHS20/10%	9.9	1.2	8.7
HMSHS30/0%	21.5	4.7	16.8
HMSHS30/3%	20.6	4.4	16.2
HMSHS30/5%	18.7	1.4	17.3
HMSHS30/10%	17.4	2.2	15.2
HMSHS40/0%	27.0	6.0	21.0
HMSHS40/3%	26.5	3.7	22.8
HMSHS40/5%	25.9	2.3	23.6
HMSHS40/10%	24.8	2.5	22.3
Nafion® 117	23.0	2.6	20.4

erally, the state of water in the membranes can be classified into three types: (i) the first type is non-freezing bound water, which is strongly associated with ionic and polar groups in the polymer chain, and cannot be detected by DSC; (ii) the second type is freezing bound water, which is defined as water weakly interacting with the polymer chain, and has a phase transition temperature of less than 0 °C; (iii) the third type is free water, which is defined as water that has the same phase transition temperature as bulk water, and that is seemingly unaffected by the polymer matrix. Generally, a low fraction of free water in membranes leads to a low electro-osmotic drag under fuel cell operation, resulting in low methanol permeability. High bound water content would be an important membrane characteristic when employed in DMFC. The free water content in the total water content was estimated using the following equation:

$$m_{\text{free}} = \frac{H_{\text{free}}}{Q_{\text{melting}}} m_{\text{total}} \quad (3)$$

Quantification of each state of water by DSC was obviously of great interest but was difficult because of the two overlapping melting peaks. Therefore, we measured the endothermic peak shown in the DSC arising from freezing water (freezing bound water and free water). Table 4 shows the water content based on total weight in HMSHS/silica nano-composite membranes corresponding to the freezing water, bound water and total water content. Fig. 5 shows the water content corresponding to the free, bound, and total water content versus degree of sulfonation. The total water and freezing water content increased linearly up to 20 mol% of sulfonic acid groups, and then sharply increased with sulfonic acid content greater than 20 mol%. The bound water increased linearly from 10 to 40 mol% of sulfonic acid groups. The percentage of freezing water abruptly increased at greater than 20 mol% sulfonic acid groups, indicating that the morphology of the membrane changed with sulfonated copolymer composition. An increase in the free volume capable of containing more water molecules, and an increase in the continuous hydrophilic domain structure, can significantly increase the water content of the copolymer. With the introduction of silica, the total water content of the HMSHS/silica nano-composite membranes decreased with increase in silica content, because inorganic nano-particles increased the bulkiness and reduce the swelling ability in the copolymer chains. It is worth noting that the freezing water increased with increase in silica content in HMSHS10/silica and HMSHS20/silica, which had a different tendency compared with HMSHS30/silica and HMSHS40/silica. In HMSHS10/silica and HMSHS20/silica membranes, the total water content decreased in the range of 11.5–7.4% and 13.8–9.9%, and the freezing water increased in the range of 0.2–0.3% and 0.2–1.2%, because of large nano-particle size and non-uniform dispersion. These give decreasing bound water of 11.3–7.1% and 13.6–8.7%. In HMSHS30/silica and HMSHS40/silica, the total water also decreased in the range of 21.5–17.4% and 27.0–24.8%. The freezing water decreased in the range of 4.7–2.2% and 6.0–2.5% from 0 to 5% silica content, and rose to 2.2% and 2.5% at 10% silica content. Because the silica content from 0 to 5% had a small nano-particle size and good dispersion in the membranes and decreased the free volume in the membranes, nevertheless, an excess of silica content in 10% rose for large nano-particle size and non-uniform dispersion could result in a counter effect. With 0–5% silica content, the bound water increased from 16.8 to 17.3% and 21.0 to 23.6% in HMSHS30/SiO_2 and HMSHS40/SiO_2, respectively. This nano-size particle behavior will be discussed further in the following section.

3.6. Proton conductivity

Fig. 6 shows the proton conductivity of HMSHS membranes as a function of temperature and degree of sulfonation. The proton conductivity of HMSHS10 to HMSHS40 membranes measured from 30 to 80 °C is 0.004–0.010, 0.017–0.038, 0.030–0.058, and 0.052–0.100 S cm^{-1}, respectively. The pro-

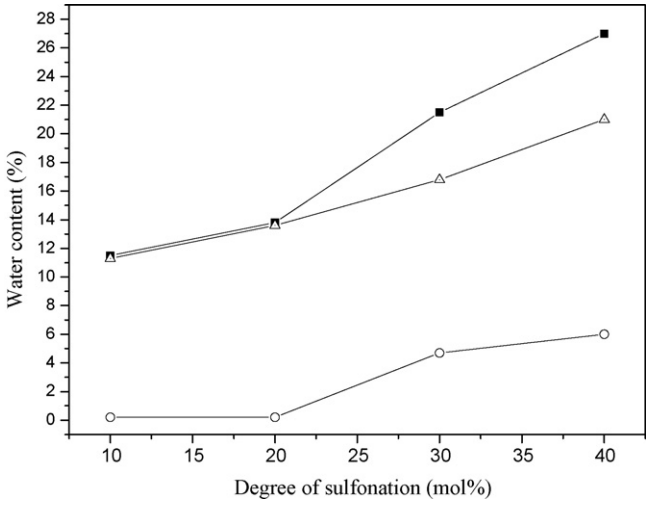

Fig. 5. The water content versus to degree of sulfonation from 10 to 40 mol%. (■) total water, (◯) free water, and (△) bound water.

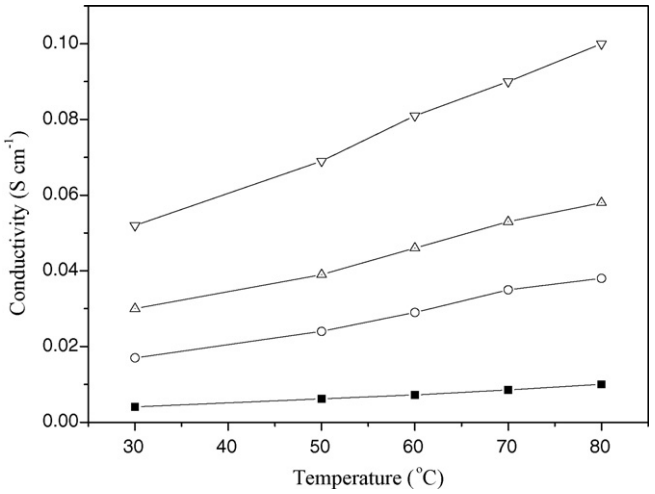

Fig. 6. The proton conductivity of HMSHS membranes as a function of temperature and degree of sulfonation: (■) HMSHS10, (◯) HMSHS20, (△) HMSHS30, and (□) HMSHS40.

ton conductivity increased with temperature and sulfonic acid content, which provided more carrier proton ions.

Fig. 7 shows the proton conductivity of HMSHS/silica nano-composite membranes with various contents of silica at 80 °C. It is apparent that the increase in silica caused a continuous decrease in conductivity in HMSHS10/silica and HMSHS20/silica. It is worth noting that for HMSHS10/silica and HMSHS20/silica membranes, the total water content decreased and the freezing water increased. These give decreasing bound water, so that the conductivity decreased in HMSHS10/silica (0.01–0.006 S cm^{-1}) and HMSHS20/silica (0.038–0.026 S cm^{-1}) with increase in silica content. In HMSHS30/silica and HMSHS40/silica, the total water also decreased and the freezing water decreased from 0 to 5% silica content, and rose at 10% silica content. Because the silica content from 0 to 5% had a small nano-particle size and good dispersion in the membranes and decreased the free volume in

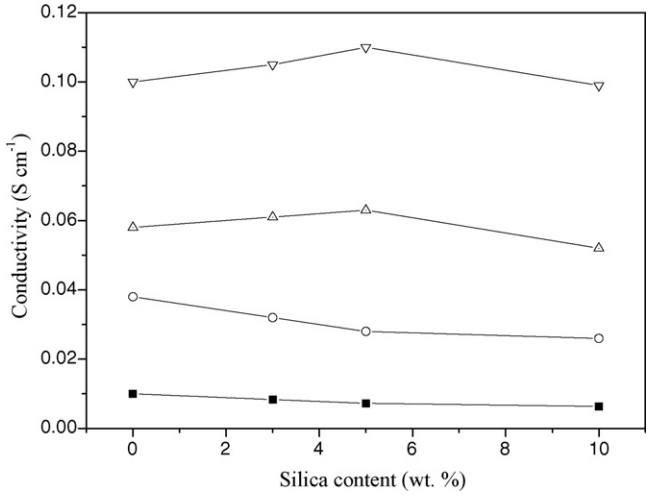

Fig. 7. The proton conductivity of the HMSHS/silica nano-composite membranes with various content of silica at 80 °C: (■) HMSHS10, (◯) HMSHS20, (△) HMSHS30, and (□) HMSHS40.

Table 5
The activation energy of the HMSHS/silica nano-composite membranes and Nafion® 117

	Activation energy, E_a (kJ mol^{-1})			
	0% silica	3% silica	5% silica	10% silica
HMSHS10	16.05	15.73	13.63	12.76
HMSHS20	14.81	12.64	11.22	9.74
HMSHS30	12.04	9.47	9.10	8.64
HMSHS40	11.77	9.37	8.01	7.37
Nafion® 117	9.28	–	–	–

the membranes, the conductivity increased in HMSHS30/silica (0.058–0.063 S cm^{-1}) and HMSHS40/silica (0.1–0.11 S cm^{-1}) with increase in silica content. Nevertheless, an excess of silica content in 10% rose for large nano-particle size and non-uniform dispersion could result in a counter effect. Compared with Nafion® 117, all HMSHS40/silica serial had much bound water, and consequently had better proton conductivity than Nafion® 117 (0.050–0.085 S cm^{-1}) of between 0.052 and 0.110 S cm^{-1}.

In general, the proton conductive mechanism in these membranes is well known to occur by two routes [3,13]: (i) the first route is a hopping or jumping mechanism, also known as the Grotthuss model; (ii) the second route is a vehicle mechanism. Therefore, the proton conductive mechanism occurs by two simultaneous routes. The activation energy (E_a), the minimum energy required for proton transport across the membrane, was calculated by fitting to the Arrhenius equation:

$$\sigma = A \times e^{-E_a/RT} \quad (4)$$

where σ is the proton conductivity (S cm^{-1}), E_a the activation energy (kJ mol^{-1}), R the universal gas constant (8.314 J mol^{-1} K^{-1}), and T is the absolute temperature (K). Activation energy values were estimated from the slopes of the plots and are summarized in Table 5. Fig. 8 shows Arrhenius plots of HMSHS40/silica nano-composite membranes. All of the HMSHS/silica membranes had a linear Arrhenius behavior between 30 and 80 °C. HMSHS/silica nano-composite mem-

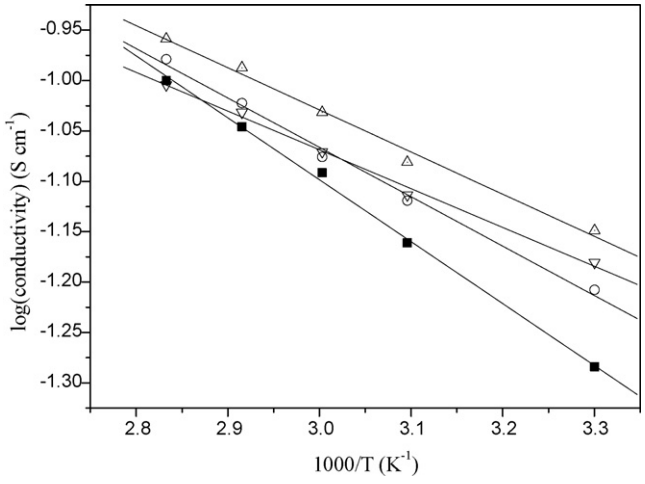

Fig. 8. Arrhenius plots of proton conductivity for the HMSHS40/silica loading with various silica contents: (■) 0%, (◯) 3%, (△) 5%, and (□) 10%.

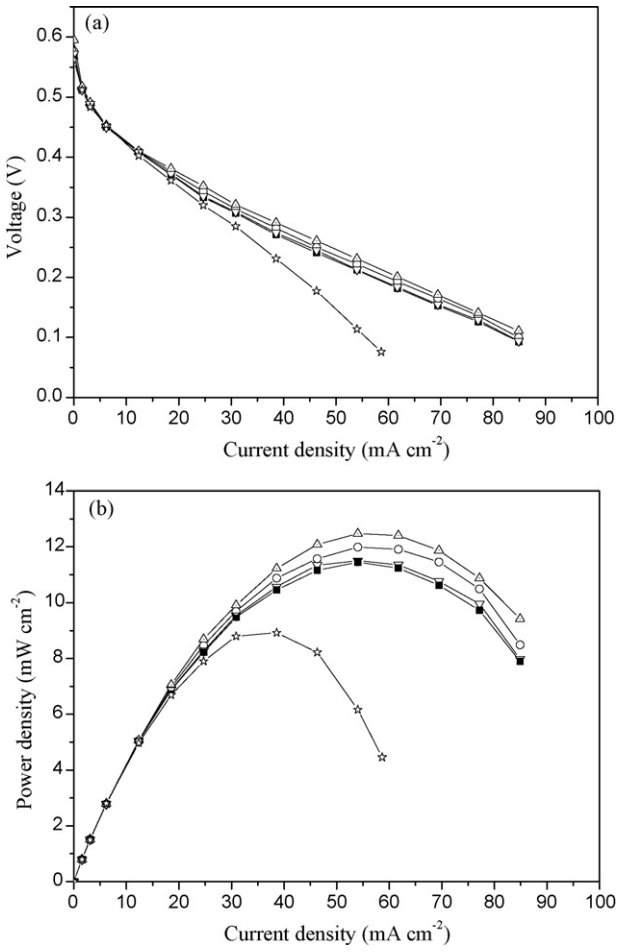

Fig. 9. The performance curve of the HMSHS40/silica and Nafion® 117 membranes: (a) Polarization curve: (■) 0%, (◯) 3%, (△) 5%, (▽) 10%, and (☆) Nafion® 117. (b) Power density curve: (■) 0%, (◯) 3%, (△) 5%, (▽) 10%, and (☆) Nafion® 117.

branes and Nafion® 117 membrane exhibited activation energies of 7.37–16.05 and 9.28 kJ mol^{-1}, respectively. For the hopping mechanism, the activation energy for proton conductivity should be around 14–40 kJ mol^{-1} and the values obtained were close to the above values [13].

3.7. Single cell performance

DMFC performance was evaluated with HMSHS40/silica and Nafion® 117 membranes. Fig. 9 shows the performance results with the polarization (a) and power density (b) as a function of current density. The cell with HMSHS40/silica nano-composite membranes had higher open circuit voltage (OCV = 0.57–0.60 V) and maximal power density than commercial Nafion® 117 (OCV = 0.56 V). The higher open circuit voltage clearly indicates that silica introduced into HMSHS40 membrane has truly decreased the rate of methanol crossover in these nano-composite membranes. The higher maximal power density indicates a better performance of HMSHS40/silica than commercial Nafion® 117. The nano-composite membrane with 5 wt.% silica loading shows a higher performance than membranes with 3 and 10 wt.%. As shown in Fig. 9, the performance of the single cell improved with increasing silica content up to 5%. With increasing the silica content to 10%, the performance of the single cell was decreased. It can be seen that the highest power density using the nano-composite membrane with 5% silicon oxide at 54 mA cm^{-2} was 12 mW cm^{-2}. On the other hand, the highest power densities of the single cell using the nano-composite membrane with 3 and 10% silica content at 54 mA cm^{-2} were 11 mA cm^{-2}. The best performance nano-composite membrane (HMSHS40/5%) had a power density of 12 mW cm^{-2} at 54 mA cm^{-2}, which was around 3 mW cm^{-2} higher than that of pure Nafion®.

4. Conclusions

In this paper, organic/inorganic nano-composite membranes have been prepared by incorporation of silica into sulfonated HMS-based PES copolymers. The membranes were characterized using ^{1}H NMR, FT-IR, SEM, TGA, DSC, water uptake, conductivity, and single cell performance. In ^{1}H NMR and FT-IR, the result proved that the sulfonate groups were indeed quantitatively introduced into the copolymers as expected. TGA and DSC measurements showed that the organic/inorganic composite membranes have good thermal properties and flexibility. SEM micrographs showed that nano-scale silica particles were uniformly distributed within the polymer matrix. The introduction of silica into composite copolymers not only enhanced the thermal properties of the composite membranes, but also improved their swelling and conductivity. Compared with Nafion® 117 membrane, the sulfonated HMS-based organic/inorganic composite membranes exhibit higher conductivity and single cell performance. The composite membranes are easy to prepare and much less expensive than the commercial Nafion® membranes. Their high conductivity and single fuel cell performance permit them to be considered for use in DMFC applications.

Acknowledgements

The authors would like to thank the National Science Council of the Republic of China for financially supporting this research under Contract No. NSC 94-2623-7-309-001-ET, and are extremely grateful to Ms. P.Y. Lin and S.C. Lan for their crucial contribution to ^{1}H NMR experiments and single cell performance tests.

References

[1] I. Honma, H. Nakajima, O. Nishikawa, T. Sugimoto, S. Nomura, Solid-State Ionics 162/163 (2003) 237–245.
[2] D.R. Vernon, F. Meng, S.F. Dec, D.L. Williamson, J.A. Turner, A.M. Herring, J. Power Sources 139 (2005) 141–151.
[3] R.K. Nagarale, G.S. Gohil, V.K. Shahi, J. Membr. Sci. 280 (2006) 389–396.
[4] J.A. Kerres, J. Membr. Sci. 185 (2001) 3–27.
[5] D.J. Jones, J.J. Roziere, J. Membr. Sci. 185 (2001) 41–58.
[6] K. Miyatake, Y. Chikashige, M. Watanabe, Macromolecules 36 (2003) 9691–9693.
[7] D. Poppe, H. Frey, K.D. Kreuer, A. Heinzel, R. Mulhaupt, Macromolecules 35 (2002) 7936–7941.

[8] F. Wang, M. Hickner, Y.S. Kim, T.A. Zawodzinski, J.E. McGrath, J. Membr. Sci. 197 (2002) 231–242.
[9] Y.S. Kim, M.A. Hickner, L. Dong, B.S. Pivovar, J.E. McGrath, J. Membr. Sci. 243 (2004) 317–326.
[10] P. Xing, G.P. Robertson, M.D. Guiver, S.D. Mikhailenko, S. Kaliaguine, Macromolecules 37 (2004) 7960–7967.
[11] P. Xing, G.P. Robertson, M.D. Guiver, S.D. Mikhailenko, S. Kaliaguine, Polymer 46 (2005) 3257–3263.
[12] W. Essafi, G. Gebel, R. Mercier, Macromolecules 37 (2004) 1431–1440.
[13] V.K. Shahi, Solid-State Ionics 177 (2007) 3395–3404.
[14] V.S. Silva, J. Schirmer, R. Reissner, B. Ruffmann, H. Silva, A. Mendes, L.M. Madeira, S.P. Nunes, J. Power Sources 140 (2005) 41–49.
[15] Y. Kim, J.S. Lee, C.H. Rhee, H.K. Kim, H. Chang, J. Power Sources 162 (2006) 180–185.
[16] R. Jiang, H.R. Kunz, J.M. Fenton, J. Power Sources 272 (2006) 116–124.
[17] V. Ganesan, A. Walcarius, Langmuir 20 (2004) 3632–3640.
[18] Y.S. Kim, L. Dong, M.A. Hickner, T.E. Glass, V. Webb, J.E. McGrath, Macromolecules 36 (2003) 6281–6285.
[19] M. Ueda, H. Toyota, T. Ochi, J. Sugiyama, K. Yonetake, T. Masuko, T. Teramoto, J. Polym. Sci. Polym. Chem. Ed. 31 (1993) 853–858.
[20] J. Mecham, H.K. Shobha, F. Wang, W. Harrison, J.E. McGrath, Polym. Preprints 41 (2000) 1388–1395.
[21] S.H. Zaheer, B. Bhushan, Nature 171 (1953) 746–747.
[22] A. Roviello, A. Sirigu, Makromol. Chem. 181 (1980) 1799–1806.
[23] V. Percec, T.D. Shaffer, H. Nava, J. Polym. Sci. Polym. Lett. Ed. 2 (1984) 637–647.
[24] C.H. Wan, J.F. Kuo, C.Y. Chen, Liq. Cryst. 27 (2000) 523–532.
[25] J. Mecham, H.K. Shobha, F. Wang, W. Harrison, J.E. McGrath, Polym. Preprints 41 (2000) 1388–1389.
[26] F. Wang, J. Mecham, W. Harrison, J.E. McGrath, Polym. Preprints 41 (2000) 1401–1402.
[27] W. Harrison, F. Wang, J. Mecham, V. Bhanu, M. Hill, Y.S. Kim, J.E. McGrath, J. Polym. Sci. Part A: Polym. Chem. 41 (2003) 2264–2276.
[28] K.B. Wiles, F. Wang, J.E. McGrath, J. Polym. Sci. Part A: Polym. Chem. 43 (2005) 2964–2976.
[29] Q. Deng, R.B. Moore, K.A. Mauritz, J. Appl. Polym. Sci. 68 (1998) 747–763.
[30] K. Prashantha, S.G. Park, J. Appl. Polym. Sci. 98 (2005) 1875–1878.